Pergamon

PII: S0191-8141(96)00105-8

Journal of Structural Geology, Vol. 19, No. 5, pp. 663 to 672, 1997

0191-8141/97 $17.00 + 0.00

Evolution of solution structures in a deformed quartz arenite: geometric changes related to permeability changes

WILLIAM M. DUNNE and ANTHONY J. CALDANARO, JR

Department of Geological Sciences, University of Tennessee, Knoxville, TN 37996, U.S.A.

(*Received* 14 *July* 1994; *accepted in revised form* 11 *November* 1996)

Abstract—Quartz arenite of the Silurian Keefer Sandstone at a site in West Virginia, U.S.A., records an early pervasive solution-related deformation by grain interpenetration. Volume losses measured by the PSS method show shortening directions from both diagenetic compaction and early tectonic layer-parallel shortening. Later solution-related tectonic deformation during folding formed transgranular stylolites along pre-existing faults or in rock volumes with abundant microfractures. Thus, the geometry of solution-related deformation changed progressively from pervasive at grain scale to focused along transgranular surfaces. We propose that this geometric change resulted from intense porosity and permeability reduction during diagenetic cementation and early layer-parallel shortening, which required fluids to exploit tectonically created pathways along faults or networks of microfractures during later deformation. © 1997 Elsevier Science Ltd.

INTRODUCTION

The purpose of this contribution is to describe the geometric and morphological changes of solution structures when a quartz sand evolves into a folded and faulted quartz arenite. The study will document a dichotomy in geometry with time. During diagenesis and early tectonic deformation, the dominant solution structure is grain interpenetration. During later tectonic deformation, transgranular stylolites develop on pre-existing faults and in rock volumes with abundant microfractures. This change in the geometry of solution-related structures means that deformation shifts from millimeter-sized features separated by millimeters to surfaces with trace lengths of 10s to 100s of centimeters and spacings of up to 10s of centimeters. Thus, solution-related deformation becomes more heterogeneous in spatial distribution and intensity with time.

Most quartz-rich rocks with sand-sized grains undergo pressure solution when deformed at less than 250°C (Groshong, 1988; Houseknecht, 1988; Knipe, 1989; Onasch, 1990, 1993, 1994; Gratz, 1991; Wu and Groshong, 1991; Lloyd and Knipe, 1992; Lundegard, 1992; Onasch and Dunne, 1993; Dewer and Hajash, 1995; Takeshita, 1995). While many factors influence the geometry of pressure solution as a deformation mechanism, the rock permeability plays a major role (Geiser and Sansone, 1981; Takeshita, 1995). The morphological changes documented in this contribution will be interpreted as relating to permeability loss during progressive deformation.

GEOLOGIC SETTING

The study area is in the eastern panhandle of West Virginia in the Valley and Ridge province of the central Appalachians (Fig. 1). The Silurian Keefer Sandstone is a thin clastic unit that is widespread across this region (Meyer *et al.*, 1992). In the study area, the dominant lithology of the sandstone consists of well-sorted, framework-supported quartz in silica cement. This monomineralic unit is typical of quartz arenites (Pettijohn *et al.*, 1987; Houseknecht, 1988). The unit is consistently 9 m thick and thickly bedded in the study area, but the thickness of the unit changes across the region with changing lithofacies (Meyer *et al.*, 1992).

The solution-related deformation of this sandstone was examined in a syncline (Fig. 1), which is parasitic to the Cacapon Mountain anticlinorium. The anticlinorium is a first-order fold in the roof sequence above a blind Alleghanian duplex (Gwinn, 1964; Rodgers, 1970; Perry, 1978; Ferrill and Dunne, 1989). The main focus of the investigation was an anticline–thrust complex within the syncline (Fig. 1). The solution-related deformation in these structures was described by constructing a 1:1000 map of the map-scale fold and fault geometries, by establishing two profiles across the complex to illustrate outcrop-scale structures and sample microscale deformation (I–I′ and O–O′ in Figs 1–3), and by establishing six representative stations for outcrop-scale and microscale structures in the syncline limbs (Stations L1 to L6 in Fig. 1). Thirty-seven samples were collected in the two profiles and syncline limbs for different types of microstructural analysis (Figs 1 & 2).

In 22 samples with over 250 counts each for microstructural abundance, subgrains, deformation lamellae and deformation bands are virtually absent (Caldanaro, 1994). Although simple undulatory extinction occurs in about 40 to 60% of grains, this microstructure may be inherited from source rocks (Pettijohn *et al.*, 1987; Onasch and Dunne, 1993), or may result from movement of only a few dislocations (Hobbs *et al.*, 1976). The lack of well-developed dislocation-related microstructures is consistent with the maximum burial temperature for the

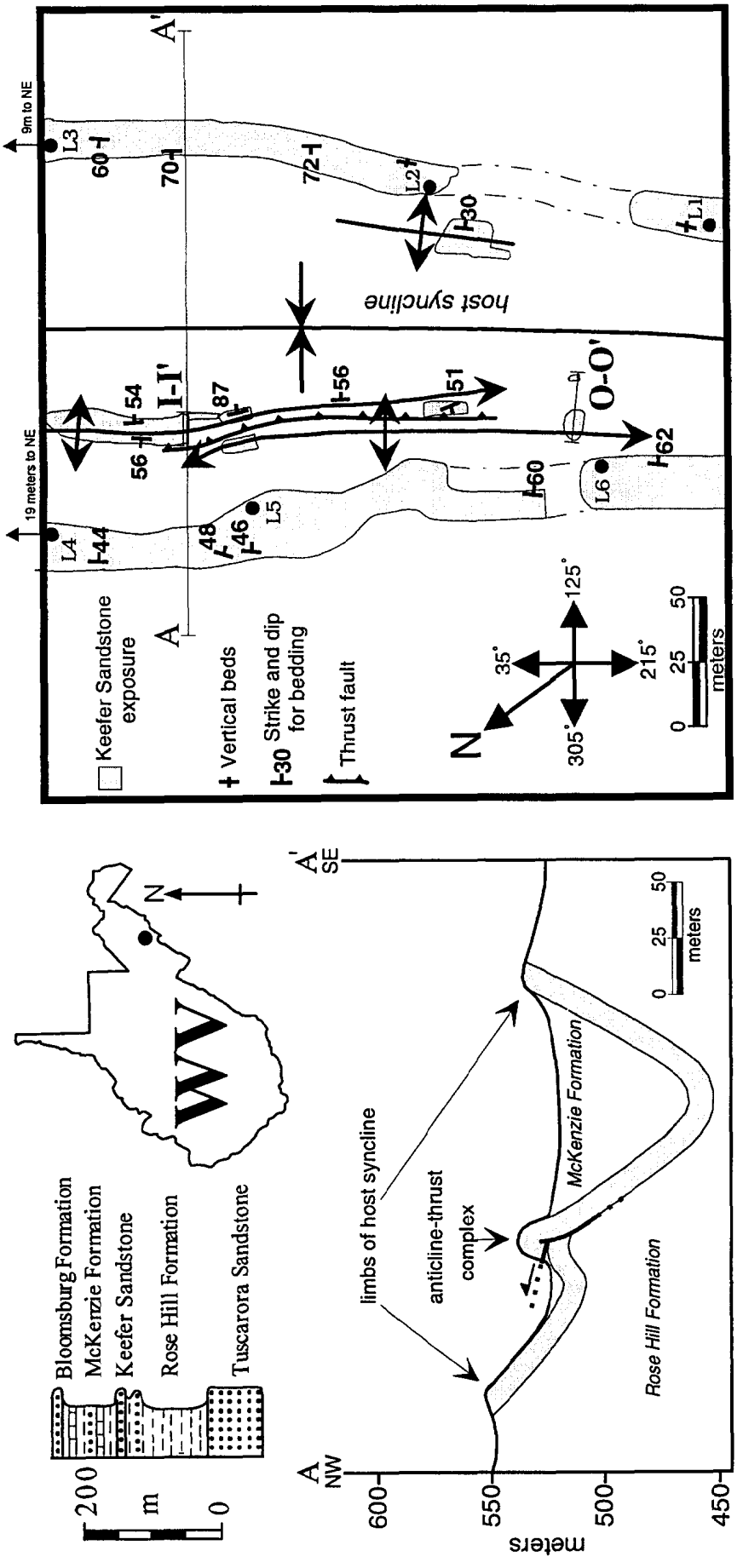

Fig. 1. Map and cross-section (A–A') of study area with Silurian stratigraphy immediately adjacent to the Keefer Sandstone. L1 to L6 with black spots are locations of samples in limbs of host syncline. Locations are shown for profiles O–O' and I–I' of Fig. 2. Approximate UTM coordinates for map center are QP00432814.

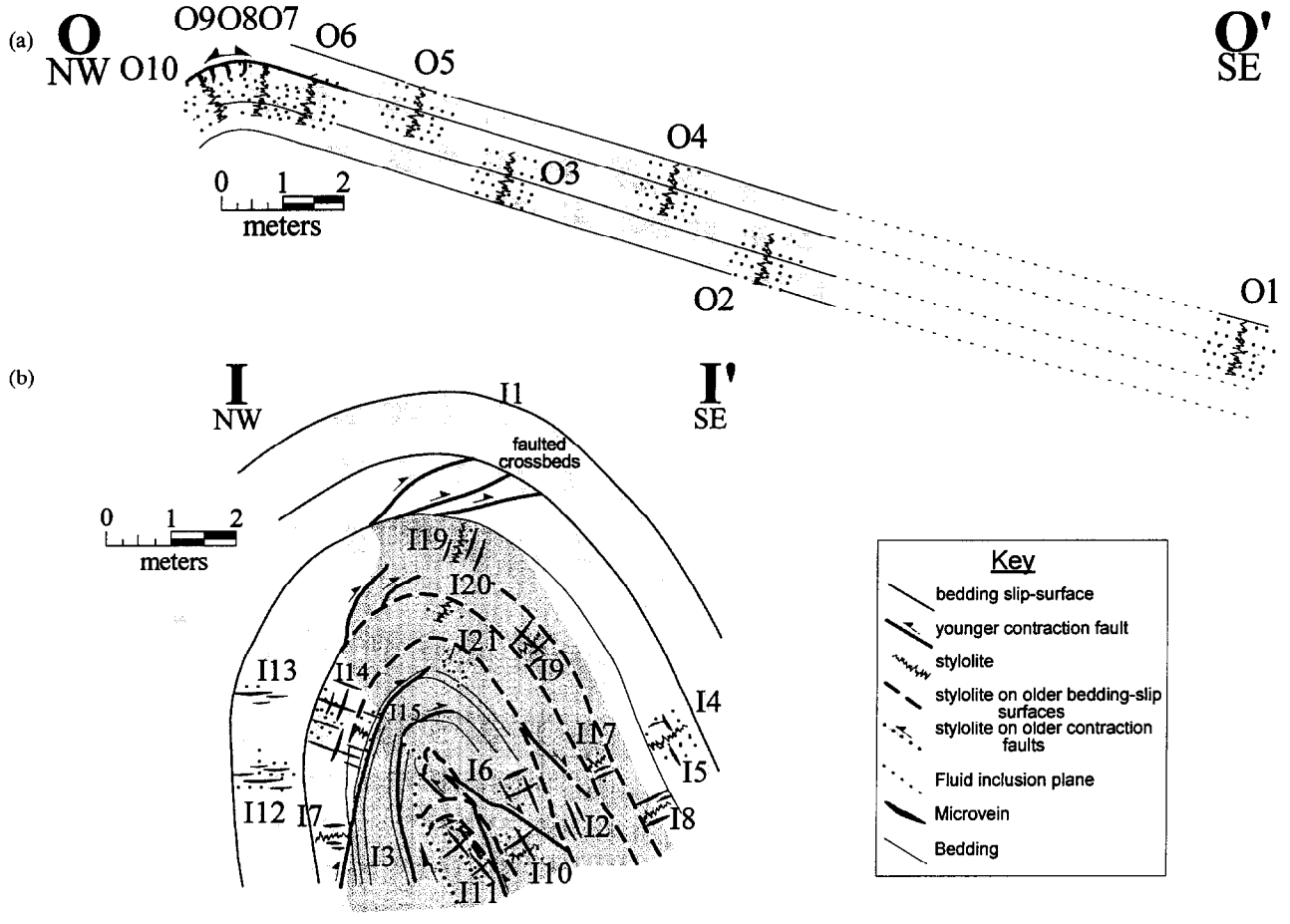

Fig. 2. Fold and fault geometries with schematic microstructural geometries and sample numbers. Each schematic representation of microstructures centers on the sample location. (a) O–O′ profile. (b) I–I′ profile. Light gray — exposed rock. Stippled region — domain of late-stage stylolites on bedding-slip surfaces and contraction faults.

Keefer Sandstone of 165–285°C (Colton, 1970; Epstein *et al.*, 1977; Onasch and Dunne, 1993; Zhang and Davis, 1993).

INTERPENETRATED GRAINS

Observations

Thirty-seven oriented samples were collected (Figs 1 & 2, Tables 1 & 2) to identify type, geometry and age relationships of microstructures and to measure volume changes. For each sample, three mutually perpendicular thin-sections were cut: parallel to bedding (*b*-section); normal to bedding and parallel to strike (*p*-section); and normal to bedding and perpendicular to strike (*v*-section). Grain-to-grain solution in the Keefer Sandstone produced ubiquitous interpenetrated grains in all 37 samples. The interpenetrations are easily visible in cathodoluminescence (Fig. 3a) because orange- and blue-luminescencing detrital quartz grains are distinguishable from dully luminescent diagenetic cement (Marshall, 1988).

The volume loss from grain-to-grain solution was determined for 18 representative samples, using the PSS strain method (Onasch, 1993, 1994) (Table 1). Only 18 samples were examined because of the large time requirement for each analysis. The method involves estimating the 'overlap quartz' in cathodoluminescence images (Fig. 3a) of interpenetrated grains by reconstructing original detrital grain boundaries, and then, measuring the volume loss (Houseknecht, 1988; Onasch, 1993). The measured loss *for each pair of grains* is a conservative estimate because: (1) a measurement is only made where a grain is clearly indented, so straight boundaries (SGB, Fig. 3a) with potentially significant solution are not used; (2) an indenting grain is treated as rigid but may have been reduced by solution; and (3) only interpenetrations between original grains can be examined, so solution of any intervening diagenetic cements is unmeasured.

The measured volume losses show: (1) shortening in all directions with an average area loss per thin section of 28%; (2) near-circular strain ellipses where only 4 of 54 have axial ratios greater than 1.1; and (3) ellipse axes that are mostly parallel to bedding strike, bedding dip direction or the normal to bedding (Table 1, Fig. 4). The last result is the most unusual. Axes of strain ellipses tend

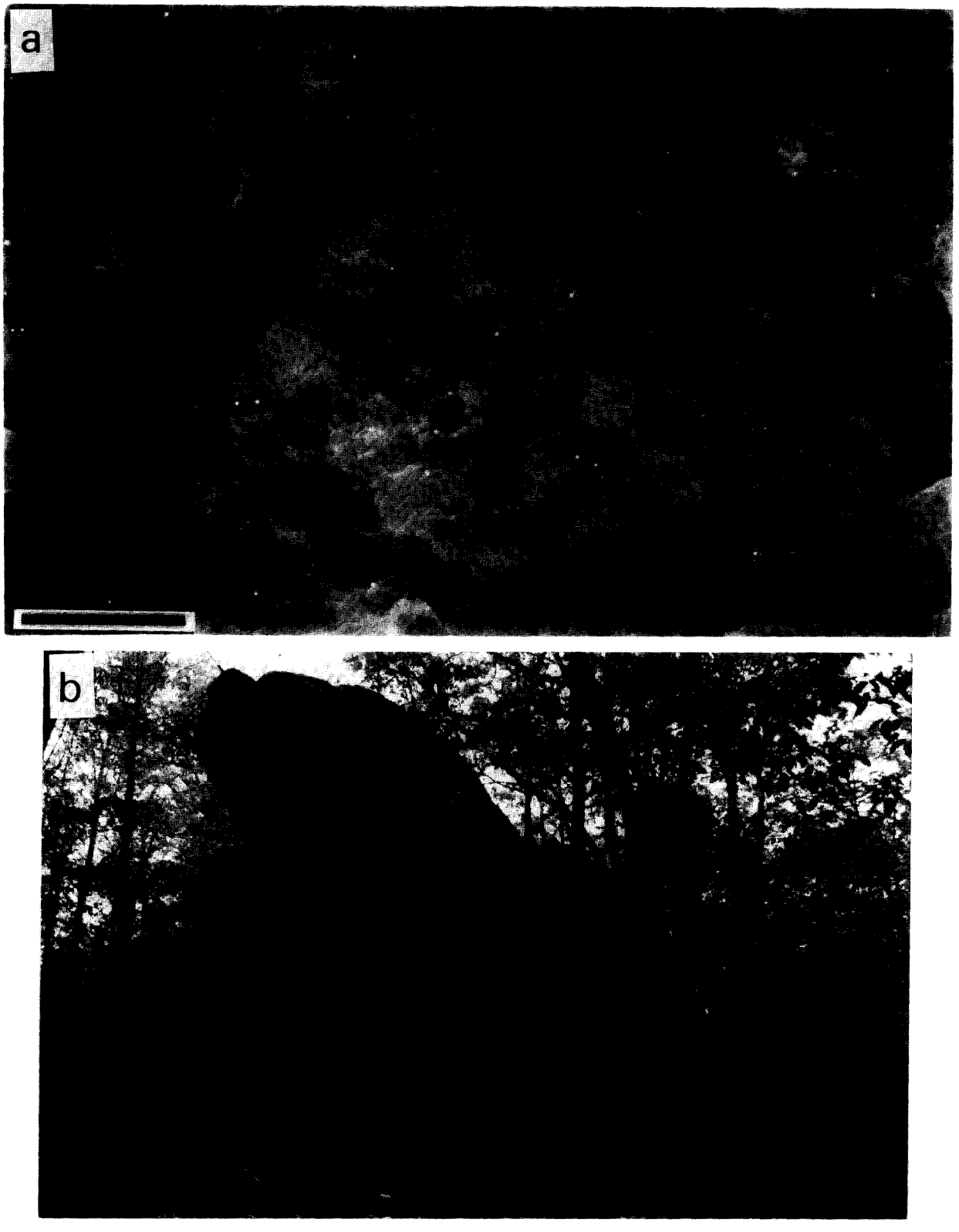

Fig. 3. Representative microstructural and outcrop-scale structural geometries. Bedding is horizontal and scale bar equals 0.5 mm in all photomicrographs. (a) Cathodoluminescent image of sample L3b, showing both grain interpenetrations (I) and straight grain boundaries (SGB). (b) I–I′ outcrop with view to the NE, profile is 8.8 m in height. (c) Multiple sets of cross-cutting, darkly luminescent microveins under CL in I15v. (d) Same view as (c) in plane-polarized transmitted light. Note bed-parallel fluid inclusion planes (FIP) cutting a microvein (MV), and bed-parallel and normal stylolites off-setting microveins; (e) Strike-parallel bed-normal stylolite (SY) in O3v. (f) Fold core at I–I′ showing prominent late-stage solution on faults and bedding (arrow points at stylolite on bedding-slip surface with 8 cm column height. Scale is 10 cm). (g) Solution pitting of bedding-slip slickenlines in SE limb of I–I′ (camera lens cap diameter is 5.2 cm).

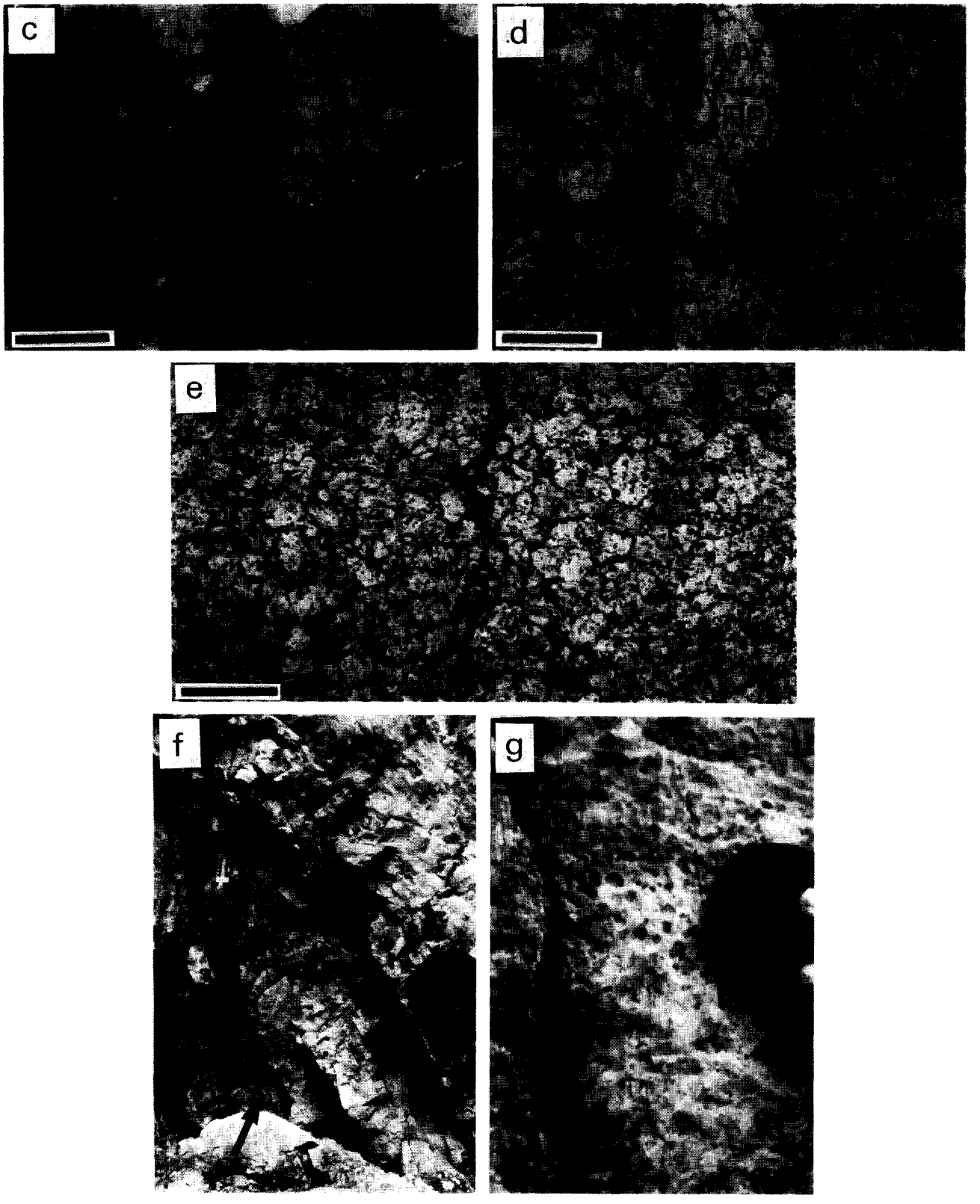

Fig. 3. (*Continued*).

Table 1. Strain ellipses measured with PSS method

Sample	*b*-section					*p*-section					*v*-section				
	Long axis	Short axis	Axial ratio	Axial rake	% Area loss	Long axis	Short axis	Axial ratio	Axial rake	% Area loss	Long axis	Short axis	Axial ratio	Axial rake	% Area loss
L1	0.90	0.81	1.11	0	27	0.90	0.83	1.08	0	25	0.83	0.81	1.02	0	33
L2	0.89	0.83	1.07	0	26	0.88	0.80	1.10	0	30	0.83	0.81	1.02	0	33
L3	0.84	0.75	1.12	0	37	0.86	0.82	1.05	0	29	0.82	0.80	1.03	0	34
O2	0.85	0.82	1.04	0	30	0.85	0.80	1.06	0	32	0.85	0.84	1.01	0	29
O3	0.83	0.81	1.02	0	33	0.87	0.76	1.14	0	34	0.84	0.76	1.11	0	36
O5	0.85	0.82	1.04	0	30	0.85	0.85	1.00	0	28	0.86	0.82	1.05	0	29
O6	0.86	0.85	1.01	0	27	0.85	0.83	1.02	0	29	0.88	0.83	1.06	0	27
O9	0.88	0.86	1.02	0	24	0.87	0.85	1.02	0	26	0.90	0.85	1.06	0	24
I4	0.87	0.85	1.02	0	26	0.88	0.85	1.04	0	25	0.85	0.85	1.00	0	28
I6	0.90	0.86	1.05	0	23	0.89	0.84	1.06	0	25	0.91	0.86	1.06	−31	22
I9	0.88	0.83	1.06	0	27	0.91	0.83	1.10	0	24	0.92	0.85	1.08	−24	22
I10	0.94	0.87	1.08	25	18	0.88	0.85	1.04	0	25	0.90	0.85	1.06	−39	24
I11	0.91	0.84	1.08	−16	24	0.91	0.85	1.07	0	23	0.90	0.85	1.06	−23	24
I12	0.89	0.83	1.07	0	26	0.87	0.82	1.06	0	29	0.89	0.83	1.07	0	26
I13	0.90	0.85	1.06	0	24	0.87	0.84	1.04	−28	27	0.88	0.82	1.07	0	28
I14	0.88	0.82	1.07	0	28	0.90	0.84	1.07	0	24	0.85	0.84	1.01	0	29
I19	0.85	0.82	1.04	0	30	0.85	0.83	1.02	0	29	0.87	0.81	1.07	0	30
I20	0.83	0.82	1.01	0	32	0.82	0.81	1.01	0	34	0.84	0.82	1.02	0	31

Rake measured from strike of section to long axis with clockwise positive.

not to be so precisely parallel from sample to sample when other techniques for finite strain measurement are applied to samples with small deformations (Couzens *et al.*, 1993; Paterson and Yu, 1994). Samples O5b, O5p, O5v and I10p in Fig. 4 have typical PSS plots for this study. Their point distributions offer no compelling evidence for constructing ellipses with long axes that have non-zero rakes (rake angle = 0 when long axes are parallel to strike in *b*-section and parallel to bedding in the *p*- and *v*-sections). A few PSS plots (e.g. I10b and I10 v in Fig. 4) do show point distributions that are not symmetric about the geometric elements of bedding, and their ellipses were constructed with non-zero rakes (Table 1). The results might be more rigorous if a least-squares regression with a filter for larger deviations was used to calculate the ellipse shapes. This approach was not used in the original method (Onasch, 1993) and is beyond the skills of the present investigators. Nevertheless, any imprecision in axial orientations does not negate the most important aspect of the measured ellipses: samples shortened in more than one direction by volume loss.

Inferences

Multiple shortening directions cannot be explained by a simple compactional event where the deformation is described by a displacement field composed of vertically

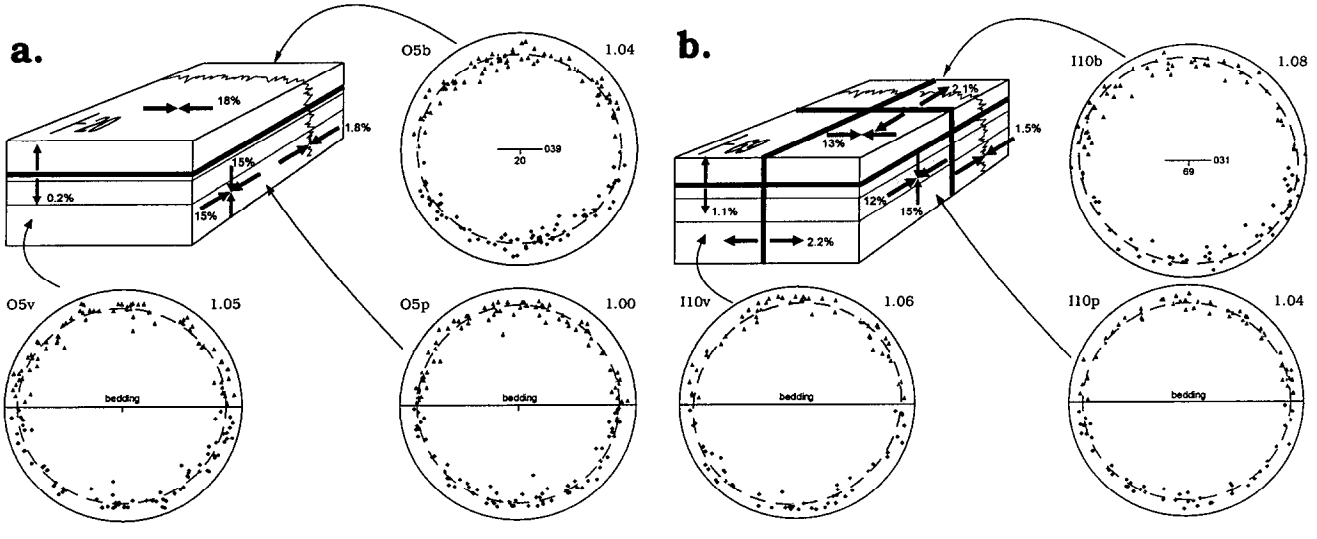

Fig. 4. Examples of PSS data with structural geometries. (a) Sample O5. (b) Sample I10. Thick black lines represent microveins and FIPs schematically. Toothed lines represent stylolites. 50 measurements were made for each PSS plot, which yields 100 points (Onasch, 1993).

oriented vectors. As Onasch (1993) observed, while simple compaction produces observable grain interpenetration in any section cut across a sample, the magnitude of volume loss is zero parallel to bedding in both *p*- and *v*-sections (e.g. Fig. 3 in Onasch, 1993). We measured volume losses parallel to bedding in the *p*- and *v*-sections of this study (Table 1, Fig. 4). Therefore, a minimum of two shortening directions is required. For most samples, the short axes of ellipses are normal to strike in the *b*-section and normal to bedding in the *p*- and *v*-sections (Table 1). These consistent geometries are interpreted as indicating that the two shortening directions were bedding-normal, and strike-normal but bedding parallel (layer-parallel shortening or LPS). Following Onasch (1993, 1994), measured shortening parallel to bedding strike is interpreted as an apparent deformation obtained from grain interpenetrations that formed by a combination of bedding-normal shortening and LPS. The temporal sequence of the two shortening directions may not be determined from PSS plots, which record a finite volume loss. LPS typically followed bed-normal diagenetic compaction for other quartz arenites of this region that deformed during the Alleghanian orogeny (Couzens *et al.*, 1993; Onasch, 1994), and that interpretation is applied here.

The four samples with ellipses that have non-zero axial rakes cannot be explained by the above proposed deformation history because they lack the appropriate axial geometries. They may represent deformation histories with more than two shortening directions (I6, I9, I10, and I11 in Table 1). This possibility is consistent with their location in the core of a collapsed isoclinal anticline (Figs 3b & 4), as will be described later.

A key issue for grain-to-grain solution is its relative timing. All transgranular microstructures, including stylolites, fluid inclusion planes (FIPs) and microveins, transect and offset interpenetrated grains (e.g. Fig. 3c). They are interpreted to postdate grain-to-grain solution. Thus, grain-to-grain solution is interpreted as the earliest deformation, accommodating diagenetic compaction and an early component of tectonic LPS.

Table 2. Volume increases by microveins and FIPs

Sample number	Microveins			%Volume increase
	Sp; b-ppd	Dp; b-ppd	Bed-par.	
L1	3.2 (0.2)		(r)	3.2
L2	1.6 (0.5)		(r)	1.6
L3	(r)		(r)	
L4	(r)			
L5	(r)			
L6	4.9 (0.2)	r		4.9
O1			(r)	
O2			(r)	
O3			0.6 (0.6)	0.6
O4			0.1 (0.1)	0.1
O5	(r)		0.2 (0.2)	0.2
O6	r	r	0.4 (0.4)	0.4
O7	6.6	0.8 (0.8)	r	7.4
O8	3.6		0.5 (0.5)	4.1
O9	5.0		0.2 (0.2)	5.2
O10	4.6	r	p	4.6
I1		0.2		0.2
I2		0.2 (0.2)	0.4	0.6
I3	0.4	3.1 (0.4)		3.5
I4		1.2 (0.3)		1.2
I5	r	4.6 (0.6)	0.5	5.1
I6	6.7 (0.1)	3.3	5.8	15.8
I7		2.6		2.6
I8	2.6	5.7 (0.5)		8.3
I9	3.6	5.7	2.3	11.6
I10	2.2 (0.2)	2.1 (0.4)	1.1 (0.1)	5.4
I11	6.3	4.2 (0.3)	9.4 (0.2)	19.9
I12	6.3 (0.5)	5.6 (0.6)		11.9
I13	1.0	0.7 (0.1)		1.7
I14	5.4	0.8 (0.8)	5.5 (1.5)	11.7
I15	7.3	3.5 (0.7)	1.4 (0.7)	12.2
I17	2.0 (0.3)	7.6 (0.7)		9.6
I19	1.6	0.8 (0.1)		2.4
I20		0.9 (0.1)	(r)	0.9
I21	0.5	2.7		3.2

Sp = strike-parallel; Dp = dip-parallel; Bed-par. = bed-parallel; b-ppd = bed-perpendicular; blank = none observed; r = rare; number = volume increase (% extension normal to walls) where number in parentheses is contribution of FIPs.

STYLOLITES

Stylolites within beds

Stylolites occur in all O–O′ and several I–I′ samples (Fig. 2). These bed-normal strike-parallel surfaces have lengths of less than 5 cm and occur within beds of 30 to 120 cm thickness. Stylolitic column amplitudes exceed grain diameters and have concentrated iron-oxide-dominated opaques (Fig. 3e).

Stylolites within beds always occur in rocks possessing microfractures (Fig. 2, Table 1 vs Table 2). Cross-cutting relationships between stylolites and fractures vary as a function of position and fracture type. FIPs are planar transgranular fractures decorated by fluid inclusions with 1 to 5 μm diameters (Laubach, 1989; Onasch, 1990; Wu and Groshong, 1991) (Fig. 3d). Microveins are also planar transgranular fractures that have greater fill widths of up to 200 μm and may lack fluid inclusions (Onasch, 1990) (Fig. 3c & d).

In the O–O′ samples, bed-parallel FIPs are always offset by microveins (Fig. 2, Table 2). In contrast, FIPs terminate at stylolites or more rarely continue across them. Thus, FIPs are interpreted as the oldest fractures, but their age relationship to the stylolites are more problematic. FIPs terminating at stylolites could mean that the FIPs are older. Yet, some FIPs terminate on the convex sides of stylolitic columns, which is a geometry that has been interpreted as indicating coeval formation of stylolites and dilatant fractures (Watts, 1983). Also, some FIPs that terminate at stylolites could be analogous to coeval process-zone fractures for stylolites in carbonate rocks (Raynaud and Carrio-Schaffhauser, 1992). The FIPs that transect stylolites postdate the stylolites. We interpret this range of age relationships between the

bed-parallel FIPs and bed-normal strike-parallel stylolites to indicate overall coeval formation, where the exact age relationship at a spot varied as a function of local propagation sequence. Simultaneous formation of these two types of structure is consistent with their geometry, because a maximum bedding-parallel compression and a minimum bedding-normal principal stress would form both.

In the I–I′ samples, the stylolites are offset by microveins and offset microveins (Fig. 3c & d). Likewise, bed-parallel FIPs are offset by microveins and transect microveins. The I–I′ profile is characterized by many sets of FIPs and microveins in different geometries that recorded volume increases of 0.2 to 19.9% with an average of 7.2% (Table 2, Figs 2–4) and mutually cross-cut each other. These fracture-related volume increases are much greater than similar increases measured in other samples except in the anticlinal hinge in the O–O′ profile (Table 2, Figs 2 & 4a vs b). Given the greater number of microfracture geometries, these increases also result from elongation in a greater number of directions than in other samples and involve more than one episode of elongation in each direction, as fracture sets mutually cross-cut. Thus, the stylolites in the I–I′ profile are interpreted to be part of a more complex deformation increment that involved multiple episodes of fracturing and stylolitization and produced an overall volume increase.

Volume losses were calculated for the stylolites by assuming that column amplitude equals width of dissolved material and that the surfaces were initially planar (Stockdale, 1926; Heald, 1955; Fletcher and Pollard, 1981; Tada and Siever, 1989). The stylolites have spacings of 3 to 5 cm, and column amplitudes of less than 1 mm, yielding an average volume loss of 1.8% for the SE limb of O–O′, 2.1% for the hinge of O–O′ and 1.5% in the I–I′ profile (Fig. 4). These values may overestimate volume loss because the stylolites were probably initially non-planar, as they presently wrap around grains rather than cutting straight across them (Fig. 3d).

Faults overprinted by stylolites

In the isoclinal anticlinal core of profile I–I′, stylolites developed on pre-existing faults, either bedding-slip surfaces or contraction faults (dark-gray region of I–I′ in Figs 2 & 3f & g). These stylolites are mostly subvertical and parallel to the axial surface of the fold. They only occur in outcrop and not at the microscale within beds. The morphology of these solution surfaces changes from the SE limb to the anticlinal core (Fig. 3g vs f). In the SE limb, the groove slickenlines of the bedding-slip surfaces are decorated by solution pits. Moving into the core, the degree of pitting and amplitude of stylolite columns increases to the point where relic faults have a stylolitic topography of several centimeters amplitude without preservation of fault-related kinematic indicators. This deformation reaches a maximum where a stylolite on a former bedding-slip surface has 8 cm of amplitude (arrow in Fig. 3f). If the volume loss was shared equally by the two adjacent beds and the slip surface was originally planar, then the stylolite caused 9% bed-normal shortening across beds that were each originally about 45 cm thick. This estimate is probably a minimum because stylolite amplitude may not represent the entire width of dissolved rock, but the initial surface was planar.

The stylolites formed on faults must be late structures because they overprint slip surfaces that were essential to the formation of the isoclinal anticline. Their location and their increasing deformation intensity into the core are interpreted to represent a flattening deformation across the anticline during the later stages of hinge collapse.

DISCUSSION

Typically, well-sorted quartz sands have initial porosities of about 40% that are eliminated by physical and chemical compaction, or cement infilling (Heald, 1956; Beard and Weyl, 1973; Houseknecht, 1987, 1988; Pettijohn *et al.*, 1987). The Keefer Sandstone has negligible present porosity and only an average of $5 \pm 2\%$ by area of former porosity replaced by diagenetic cement per sample (Table 3). We interpret this porosity elimination to result from grain interpenetration, which removed portions of grains, removed portions of cement and allowed pores to close by grain-boundary sliding. Thus, the grain-to-grain solution and diagenetic cementation would have effectively sealed the quartz arenite of the Keefer Sandstone.

One artifact of this sealing was the reactivation of faults as stylolites during later deformation. Fault surfaces apparently provided conduits for fluid flow and were favorably oriented in the anticlinal core of the I–I′ profile, where they became shortening sites for stylolitization. Since the surfaces were not very common, individually they recorded much large volume losses than pairs of interpenetrated grains or other stylolites. Thus, the deformation heterogeneity was enhanced by limiting the number of fluid pathways.

Still, the rocks of the O–O′ and I–I′ profiles do contain bed-normal stylolites that postdate the grain-to-grain solution event. These structures do require fluid flux through the sandstone, which is apparently inconsistent with our belief that the grain-to-grain solution event sealed the quartz arenite. One possible explanation for the existence of these stylolites is that not all the surviving 5% porosity in the Keefer Sandstone was cemented during grain-to-grain solution. The cement and vein infills are both dully luminescent in cathodoluminescence, so their relative ages cannot be distinguished, allowing for this possibility. A more interesting explanation is based on two observations: (1) stylolites within beds always occur with microfractures; and (2) the stylolites in the I–I′ profile record more than one episode of activity where the microfractures also record repeated

Table 3. Percentage of silica cement in quartz arenite samples

Sample	*b*-section	*v*-section
L1	3.0	2.5
L2	3.0	3.5
L3	5.0	4.0
L4	3.5	2.5
L5	4.0	0.0
L6	2.5	2.5
O1	2.0	4.0
O2	6.0	7.5
O3	5.5	4.0
O4	3.5	2.0
O5	5.0	4.5
O6	3.5	6.0
O7	4.0	3.5
O8	5.5	1.5
O9	5.5	3.0
O10	2.5	3.0
M1	8.5	5.0
M2	7.5	9.0
M3	9.0	7.5
M4	5.0	5.0
M5	0.5	2.5
M6	7.0	5.0
M7	4.5	4.5
M8	6.0	5.5
M9	4.5	3.0
M10	4.0	6.5
I1	4.5	5.0
I2	3.0	4.0
I3	6.0	3.5
I4	3.5	7.0
I5	5.0	3.0
I6	6.0	3.5
I7	5.0	3.0
I8	n/m	n/m
I9	7.5	5.5
I10	4.5	4.0
I11	4.0	6.0
I12	4.0	3.0
I13	2.5	4.5
I14	5.5	5.5
I15	8.5	7.5
I17	5.5	7.0
I19	n/m	n/m
I20	n/m	n/m
I21	n/m	n/m

n/m—not measured, based on 200 counts per thin-section.

fracturing. We suggest that the fluids necessary for stylolite formation were only able to enter the 'sealed' quartz arenite by exploiting pathways created by microfractures. Where fracture pathways could remain open, as in the complex fracture networks of the I–I′ profiles, the stylolites could continue to receive fluids and be reactivated. In fact, the strain ellipses measured in the I–I′ profile with non-zero rakes may indicate that microfracture pathways were so abundant that even some grain-to-grain solution could occur again.

Finally, we wish to emphasize the dichotomy of solution structures with time. Initially, solution was distributed through the Keefer Sandstone at the grain-scale, accommodating diagenetic compaction and LPS via grain interpenetration. After this deformation and cementation sealed the quartz arenite, subsequent solution occurred along much less abundant and much larger transgranular stylolites. We believe this change in structural morphology reflects the step-like change from a rock deforming with a pervasive porosity and fluid flux to one that needed fracture porosity to create local fluid pathways for solution deformation.

Acknowledgements—This work was partially funded by NSF grants EAR-8915949 and EAR-9206617 to Dunne, and grants-in-aid from the Geological Society of America, the American Association of Petroleum Geologists and Sigma Xi to Caldanaro. We would like to thank B. Couzens, R. Hatcher Jr, B. Price, K. Smart, R. Williams, S. Wojtal, N. Woodward, M. McNaught and an anonymous referee for providing helpful insights and comments. C. Onasch is also thanked for his comments, preprints of his PSS method, and for help with sample preparation and the cathodoluminoscope. R. Sepanski is thanked for producing the photographs. B. Couzens, M. Green, G. Yanagihara and B. Glumac are thanked for field assistance. RaNaye Dreier is thanked for an internship at ORNL for Caldanaro. We would also like to thank the Dyer family of Wardensville, WV, for access to their property.

REFERENCES

Beard, D. C. and Weyl, P. K. (1973) Influence of texture on porosity and permeability of unconsolidated sand. *Bulletin of the American Association of Petroleum Geologists* **57**, 349–369.

Caldanaro, A. J. (1994) Trading space for time: An example of fold development from the central Appalachians. Unpublished MSc thesis, University of Tennessee, Knoxville, U.S.A.

Colton, G. W. (1970) The Appalachian basin — its depositional sequences and their geologic relationships. In *Studies of Appalachian Geology: Central and Southern*, eds G. W. Fischer, F. J. Pettijohn, J. C. Read, Jr and K. N. Weaver. Wiley–Interscience, New York.

Couzens, B. A., Dunne, W. M., Onasch, C. M. and Glass, R. (1993) Strain variations and three-dimensional strain factorization at the transition from the southern to central Appalachians. *Journal of Structural Geology* **15**, 451–464.

Dewer, T. and Hajash, A. (1995) Rate laws for water-assisted compaction and stress-induced water–rock interaction in sandstones. *Journal of Geophysical Research* **100**, 13093–13112.

Epstein, A. G., Epstein, J. B. and Harris, L. D. (1977) Conodont color alteration — an index to organic metamorphism. *Professional Paper of the US Geological Survey* **995**.

Ferrill, D. A. and Dunne, W. M. (1989) Cover deformation above a blind duplex: an example from West Virginia, U.S.A. *Journal of Structural Geology* **11**, 421–431.

Fletcher, R. C. and Pollard, D. D. (1981) Anticrack model for pressure solution surfaces. *Geology* **9**, 419–424.

Geiser, P. A. and Sansone, S. (1981) Joints, microfractures, and the formation of solution cleavage in limestone. *Geology* **9**, 280–285.

Gratz, A. J. (1991) Solution-transfer compaction of quartzites; progress toward a rate law. *Geology* **19**, 901–904.

Groshong Jr, R. H. (1988) Low-temperature deformation mechanisms and their interpretations. *Bulletin of the Geologogical Society, America* **100**, 2025–2038.

Gwinn, V. E. (1964) Thin-skinned tectonics in the Plateau and northwestern Valley and Ridge province of the central Appalachians. *Bulletin of the Geological Society, America* **75**, 863–900.

Heald, M. T. (1955) Stylolites in sandstones. *Journal of Geology* **63**, 101–114.

Heald, M. T. (1956) Cementation of Simpson and St Peter sandstones I: parts of Oklahoma, Arkansas, and Missouri. *Journal of Geology* **64**, 16–30.

Hobbs, B. E., Means, W. D. and Williams, P. F. (1976) *An Outline of Structural Geology*. John Wiley and Sons, Inc., New York.

Houseknecht, D. W. (1987) Assessing the relative importance of compaction processes and cementation to reduction of porosity in sandstones. *Bulletin of the American Association of Petroleum Geologists* **71**, 633–642.

Houseknecht, D. W. (1988) Intergranular pressure solution in four quartzose sandstones. *Journal of Sedimentary Petrology* **58**, 228–246.

Knipe, R. J. (1989) Deformation mechanisms — recognition from natural tectonites. *Journal of Structural Geology* **11**, 127–146.

Laubach, S. E. (1989) Paleostress directions from the preferred orientation of closed microfractures (fluid-inclusion planes) in sandstone, East Texas basin, U.S.A. *Journal of Structural Geology* **11**, 603–611.

Lloyd, G. E. and Knipe, R. J. (1992) Deformation mechanisms accommodating faulting of quartzite under upper crustal conditions. *Journal of Structural Geology* **14**, 127–143.

Lundegard, P. D. (1992) Sandstone porosity loss — A 'big picture' view of the importance of compaction. *Journal of Sedimentary Petrology* **62**, 250–260.

Marshall, D. J. (1988) *Cathodoluminescence of Geological Materials*. Unwin Hyman, Boston.

Meyer, S. C., Textoris, D. A. and Dennison, J. M. (1992) Lithofacies of the Silurian Keefer Sandstone, east-central Appalachian basin, U.S.A. *Sedimentary Geology* **76**, 187–206.

Onasch, C. M. (1990) Microfractures and their role in deformation of a quartz arenite from the central Appalachian foreland. *Journal of Structural Geology* **12**, 883–894.

Onasch, C. M. (1993) Determination of pressure solution shortening in sandstones. *Tectonophysics* **227**, 145–159.

Onasch, C. M. (1994) Assessing brittle volume-gain and pressure solution volume-loss processes in quartz arenite. *Journal of Structural Geology* **16**, 519–530.

Onasch, C. M. and Dunne, W. M. (1993) Variation in quartz arenite deformation mechanisms between a roof sequence and duplexes. *Journal of Structural Geology* **15**, 465–475.

Paterson, S. R. and Yu, H. (1994) Primary fabric ellipsoids in sandstones: implications for depositional processes and strain analysis. *Journal of Structural Geology* **16**, 505–517.

Perry, W. J. (1978) Sequential deformation in the central Appalachians. *American Journal of Science* **278**, 518–542.

Pettijohn, F. J., Potter, P. E. and Siever, R. (1987) *Sand and Sandstone*. Springer-Verlag, New York.

Raynaud, S. and Carrio-Schaffhauser, E. (1992) Rock matrix structures in a zone influenced by a stylolite. *Journal of Structural Geology* **14**, 973–979.

Rodgers, J. (1970) *The Tectonics of the Appalachians*. Wiley–Interscience, New York.

Stockdale, P. B. (1926) The stratigraphic significance of solution in rocks. *Journal of Geology* **34**, 399–414.

Tada, R. and Siever, R. (1989) Pressure solution during diagenesis. *Annual Reviews of Earth and Planetary Science* **17**, 89–118.

Takeshita, T. (1995) Dynamic analysis of deformed quartz grains from the folded middle Miocene Momonoki Subgroup of central Japan; origin of healed microcracks. *Tectonophysics* **245**, 277–297.

Watts, N. L. (1983) Microfractures in chalks of Albuskjell Field, Norwegian Sector, North Sea: Possible origin and distribution. *Bulletin of the American Association of Petroleum Geologists* **67**, 201–234.

Wu, S. and Groshong, R. H. Jr (1991) Low-temperature deformation of sandstone, southern Appalachian fold–thrust belt. *Bulletin of the Geological Society, America* **103**, 861–875.

Zhang, E. and Davis, A. (1993) Coalification patterns of the Pennsylvanian coal measures in the Appalachian foreland basin, western and south-central Pennsylvania. *Bulletin of the Geological Society, America* **105**, 162–174.